Overlapping faults and their effect on fluid flow in different reservoir types: A LIDAR-based outcrop modeling and flow simulation study

Atle Rotevatn, Simon J. Buckley, John A. Howell, and Haakon Fossen

ABSTRACT

In this article we focus on the potential of fault-overlap zones as conduits for fluid flow in a variety of reservoir types. Light detection and ranging (LIDAR) technology were applied to collect a three-dimensional, spatially constrained data set from a well-exposed fault-overlap zone that crops out in the Devil's Lane area of the Canyonlands National Park in Utah. A virtual outcrop was generated and used to extract structural and stratigraphic data that were taken into a reservoir modeling software and reconstructed. The outcrop-based model was flow simulated and used to test fluid flow through a real-world fault-overlap zone. A structural framework was built based on collected outcrop data and combined with a series of nine different facies models. The different facies models included an eolian model based on the outcrop and a range of synthetic fluvial and shallow marine systems. Results show that, for certain depositional models, cross-fault reservoir communication may be poor despite the geometric connectivity of the relay beds. This was the case for low net/gross fluvial models and shoreface models. Conversely, high net/gross fluvial systems and eolian systems show good communication through the same relay zone. Overall, the results show that, in the presence of a fault-overlap zone, pressure communication across a relay ramp

Manuscript received August 17, 2007; provisional acceptance November 7, 2007; revised manuscript received August 30, 2008; final acceptance September 30, 2008.
DOI:10.1306/09300807092

AUTHORS

ATLE ROTEVATN ~ *Center for Integrated Petroleum Research and Department of Earth Science, University of Bergen, Allégaten 41, 5007 Bergen, Norway; present address: Rocksource ASA, P.O. Box 994 Sentrum, 5808 Bergen, Norway; atle.rotevatn@rocksource.com*

Atle Rotevatn received his Candidatus Scientiarum degree (M.Sc. degree equivalent) from the University of Oslo in 2004, studying ductilely deformed rocks of the East Greenland Caledonides. In 2007, he received his Ph.D. in structural geology from the University of Bergen, focusing on reservoir-scale deformation structures and their influence on fluid flow in oil and gas reservoirs. In 2006, he joined the Norwegian exploration and production company Rocksource where he currently works in international exploration.

SIMON J. BUCKLEY ~ *Center for Integrated Petroleum Research, University of Bergen, Allégaten 41, 5007 Bergen, Norway*

Simon Buckley received his B.Sc. degree (1999) and Ph.D. (2003) in geomatics from Newcastle University, United Kingdom. He has since been a research fellow at the University of Newcastle, Australia, and is currently a researcher at the University of Bergen. His research interests include the application and advancement of geomatics techniques, particularly LIDAR and photogrammetry, within the earth sciences.

JOHN A. HOWELL ~ *Center for Integrated Petroleum Research, University of Bergen, Allégaten 41, 5007 Bergen, Norway*

John Howell holds a B.Sc. degree (hons) from the University of Wales and a Ph.D. (1992) from the University of Birmingham (United Kingdom). After working 10 yr at the University of Liverpool, he established the virtual outcrop geology group at the Center for Integrated Petroleum Research (University of Bergen). His current research interests include collection and use of virtual outcrop data. He divides his time between the University and Rocksource, which he cofounded.

HAAKON FOSSEN ~ *Center for Integrated Petroleum Research, University of Bergen, Allégaten 41, 5007 Bergen, Norway*

Haakon Fossen received his Candidatus Scientiarum degree (M.Sc. degree equivalent) from the University of Bergen (1986) and his Ph.D. in structural geology from the University of Minnesota (1992). He joined Statoil in 1986 and, since 1996, has been a professor in structural geology at the University of Bergen. His scientific interests cover the evolution and collapse of mountain ranges, the structure of rift basins, and petroleum-related deformation structures at various scales.

ACKNOWLEDGEMENTS

Jan Tveranger is thanked for technical help in the reservoir modeling process. Sigurd Aanonsen and Elisabeth Dale are acknowledged for advice on reservoir engineering issues and the dynamic parameters used as input in the flow simulation. StatoilHydro provided the aerial photo used in Figures 2a and 4b. Figure 1 was reproduced with permission from Elsevier. The authors thank Andy Fry for logistical support in Utah and Betty Riegl for her tireless efforts in the field. Riegl Laser Measurement Systems GmbH is acknowledged for providing software support. The manuscript has benefited greatly from the constructive input of reviewers S. E. Laubach, P. Kaufman, C. Hermanrud, and editor G. M. Gillis. The work presented in this study was funded by the Norwegian Research Council's Petromax program under the umbrella of the Virtual Outcrop Geology and Fault Facies projects.

may still be poor depending on the scale of the faults and relay ramp as well as the geometry and volume of the sands.

INTRODUCTION

Faults commonly constitute barriers or baffles that obstruct or divert the flow of fluids in subsurface hydrocarbon reservoirs during production (e.g., Knipe, 1997; Fisher and Knipe, 2001; Sorkhabi and Tsuji, 2005). Fault evolution is associated with the nucleation, growth, and linkage of fault segments during progressive deformation (Cartwright et al., 1996). The linkage of segments is associated with zones of fault overlap and the formation of relay ramps (e.g., Peacock and Sanderson, 1994; Childs et al., 1995; Mansfield and Cartwright, 2001). Relay ramps develop as fault segments link up from an initial soft-linked relay between overlapping faults to a breached relay (hard link) when the segments eventually coalesce (Peacock and Sanderson, 1991). In petroleum reservoirs, soft-linked relays are known to be associated with the preservation of geometric connectivity between reservoir zones that are otherwise breached by faulting and may represent conduits for fluid flow (Hesthammer and Fossen, 1997; Manzocchi et al., 2004; Rotevatn et al., 2007). However, the details of how overlapping fault systems affect flow dynamics remain relatively poorly understood. In particular, there is a gap in our understanding of how the depositional facies of a reservoir influences the way in which fluid flow is affected by overlapping faults. This is the focus of the current article, in which we aim to contribute to fill this gap. Several of the main challenges addressed in this article follow:

1. How do overlapping faults affect fluid flow in reservoirs formed in different depositional environments?
2. How do overlapping faults affect fluid flow in reservoirs with different depositional dip directions, relative to the orientation of the fault system itself?
3. How do overlapping faults affect fluid flow in reservoirs with different net/gross ratios?

Herein we present work that combines geological field data with synthetic depositional models, which have been merged into a reservoir modeling and fluid-flow simulation study. An overlapping fault system in Canyonlands National Park (Utah) forms the basis for the field data set, which in turn is used to build a three-dimensional (3-D) geocellular model based on the outcrop. After populating the reservoir model with stochastic

and deterministic facies, we perform fluid-flow simulation to dynamically address the issues listed above.

METHODOLOGY: LIDAR SCANNING AND OUTCROP MODELING

The use of analogs is fundamental in geology, especially for geologists working with spatially limited or low-resolution subsurface data sets. Systematic and appropriately targeted outcrop studies provide a much greater control on geological detail than is possible from subsurface data because they provide far better vertical resolution than seismic data and better lateral information than spatially restricted, one-dimensional borehole-derived logs and cores. Three-dimensional geocellular models are now the established method for representing and investigating subsurface reservoirs (Flint and Bryant, 1993; Grammer and Eberlli, 2004), both statically (volumes, connectivity, geometry, etc.) and dynamically (simulating fluid flow). The generation of geocellular models is based on the mapping of seismic surfaces to produce zones, which are then filled with cells. Cells are populated with properties (such as porosity, permeability, facies, etc.), which are sampled at the wells and interpolated between them. Because wells are typically widely spaced (~0.4 km [0.2 mi] onshore; >1 km [0.6 mi] offshore), such interpolation is subject to a wide degree of uncertainty, especially in structural studies where vertical and subvertical wells are typically targeted away from large faults and rarely hit smaller subseismic ones by chance. Geostatistical data from reservoir analogs are commonly used to fill in the blanks between wells in the subsurface reservoir. Taking it a step further, reservoir models of outcrop analogs (outcrop models), used to gain insight into specific reservoir types and forming a base for generic models, have been widely used in industry and academia for the last 10–15 yr (Dreyer et al., 1993; Flint and Bryant, 1993; Bryant et al., 2000; Howell and Flint, 2002; Hodgetts et al., 2004; Pringle et al., 2004b; Pringle et al., 2006; Howell et al., in press). Through the investigation of a multitude of geological scenarios, outcrop modeling has yielded a greater appreciation of the importance of geological detail and has greatly improved and directly influenced the industry standards for building reservoir models. Traditionally, outcrop modeling involves low-tech data collection methods such as sedimentary logging, photo logs, and geological mapping. In the current study, terrestrial light detection and ranging (LIDAR) data have been collected and used as the basis for building a 3-D geocellular model of a structurally complex outcrop analog in Canyonlands National Park, Utah.

Terrestrial laser scanning (also known as LIDAR) is a well-established technology for creating 3-D reconstructions of real objects. This technology can be used for a variety of scientific as well as industrial purposes, such as entertainment (creating 3-D models for movies and video games), architecture and heritage recording (e.g., scanning buildings for the historical record), art conservation (e.g., scanning sculptural artwork) (Levoy et al., 2000), mining (stockpile volumes), reverse engineering (obtaining ''as-built'' plans), and many more. Terrestrial laser scanning has only recently been introduced in geological fieldwork, and a small number of articles describing the technology (Pringle et al., 2004a; McCaffrey et al., 2005; Waggot et al., 2005; Enge et al., 2007; Buckley et al., 2008) and a few field-based studies (Pringle et al., 2004b; Bellian et al., 2005) exist. The method is, however, gaining popularity among geoscientists because of its accuracy, resolution, and ability to record a large amount of data in a relatively short time.

Previous geoscientific studies using LIDAR (Pringle et al., 2004b; Bellian et al., 2005) have been focused on stratigraphic modeling. To date, there have been fewer published studies on the use of LIDAR data sets for addressing structural issues with the exception of a recent detailed survey of fault surface topography in the western United States (Sagy et al., 2007) and popular science articles on northwestern England (Clegg et al., 2005) and northern Norway (Wilson et al., 2005). The current article makes use of LIDAR technology in the collection and extraction of structural geological data, which in turn are used to generate a 3-D geocellular model of a structurally complex reservoir analog.

FIELD AREA AND GEOLOGICAL BACKGROUND

The Devil's Lane is located in the northern part of the Grabens region in the Needles, Canyonlands National Park, southeast Utah (Figure 1). As the name suggests, the Grabens region of Canyonlands is a heavily faulted area, which has undergone deformation throughout the last 15 m.y. because of the regional uplift of the Colorado Plateau and the collapse of a subsurface layer of salt (e.g., Davis, 1999). The uplift caused the exhumation of the current surface level, during which the crust cooled, resulting in pervasive tension fracturing as the rocks rose to the surface. Coevally, the Colorado River, just west of today's Grabens area, eroded a deep canyon into the uplifting plateau, eventually cutting down into the Pennsylvanian Paradox Formation. The Paradox Formation includes significant evaporate deposits and is extensively distributed in the Colorado Plateau. As the Colorado River brought the groundwater table into contact with the salt layer, the salt layer was destabilized and dissolved, causing the fractured crust above to collapse (e.g., Baars, 2003). As the crust collapsed, the existing tension fractures represented weaknesses along which deformation could be accommodated. Therefore, the tension fractures were reactivated as extensional faults (Moore and Schultz, 1999). As the collapse of the crust above the unstable salt progressed, an array of overlapping fault systems was formed in what is today known as the Grabens area in Canyonlands National Park. This process is still ongoing.

The heavily faulted area features a series of interconnected systems of horsts and grabens (e.g., Trudgill and Cartwright, 1994) and a configuration of faults and fault blocks that is geometrically analogous to many subsurface hydrocarbon reservoirs, e.g., in the North Sea. The host rock to the faulting is the predominantly eolian, Permian-age Cedar Mesa Sandstone (Mountney, 2004). The area chosen for the data collection in the current study was the graben system in the Devil's Lane, which features a right-lateral step, or shift, of the bounding faults, resulting in a right-lateral step of the entire graben (Figure 2a). This type of stepping or shifting is common in graben systems and is related to the faults' evolution through segment growth and linkage. In the stepover area, the bounding faults constrain two oppositely dipping relay ramps with numerous smaller faults. The full structural complexity of this outcrop has been mapped (using LIDAR) and replicated in a 3-D geocellular outcrop model.

WORK FLOW: FROM FIELD DATA TO THE VIRTUAL OUTCROP

Field Data Collection using LIDAR Scanning

Data collection was conducted using methods and workflows described in detail by Enge et al. (2007) and Buckley et al. (2008). Herein, a brief summary is given.

Terrestrial laser scanning data are combined with digital imagery and GPS to collect high-resolution, high-precision digital outcrop data. In the current study, a Riegl LMS-Z420i scanner was used to acquire a 3-D point data set from the outcrop. The 3-D point data are recorded based on the traveltime of the laser from the scanner to the target, the orientation of the laser beam (angles from vertical and horizontal starting point), and the strength of laser return (intensity). In its simplest form, the recorded data can be represented by xyz format.

A total of 13 overlapping scans were collected throughout the locality over a period of 2 days (Figure 2a). Because the main aim of the data collection was to obtain a structural data set, the scanning was focused on the faults, relay ramps, and associated smaller structural elements (Figure 3). The merged point cloud from the 13 scans is shown in Figure 2b and c.

Data Processing and Generation of the Virtual Outcrop

Point cloud data represent millions of 3-D points. For stratigraphic studies, the interpretation is commonly made directly on to the point cloud (Bellian et al., 2005). However, application of the point cloud for structural studies is more problematic because features such as cracks, joints, deformation

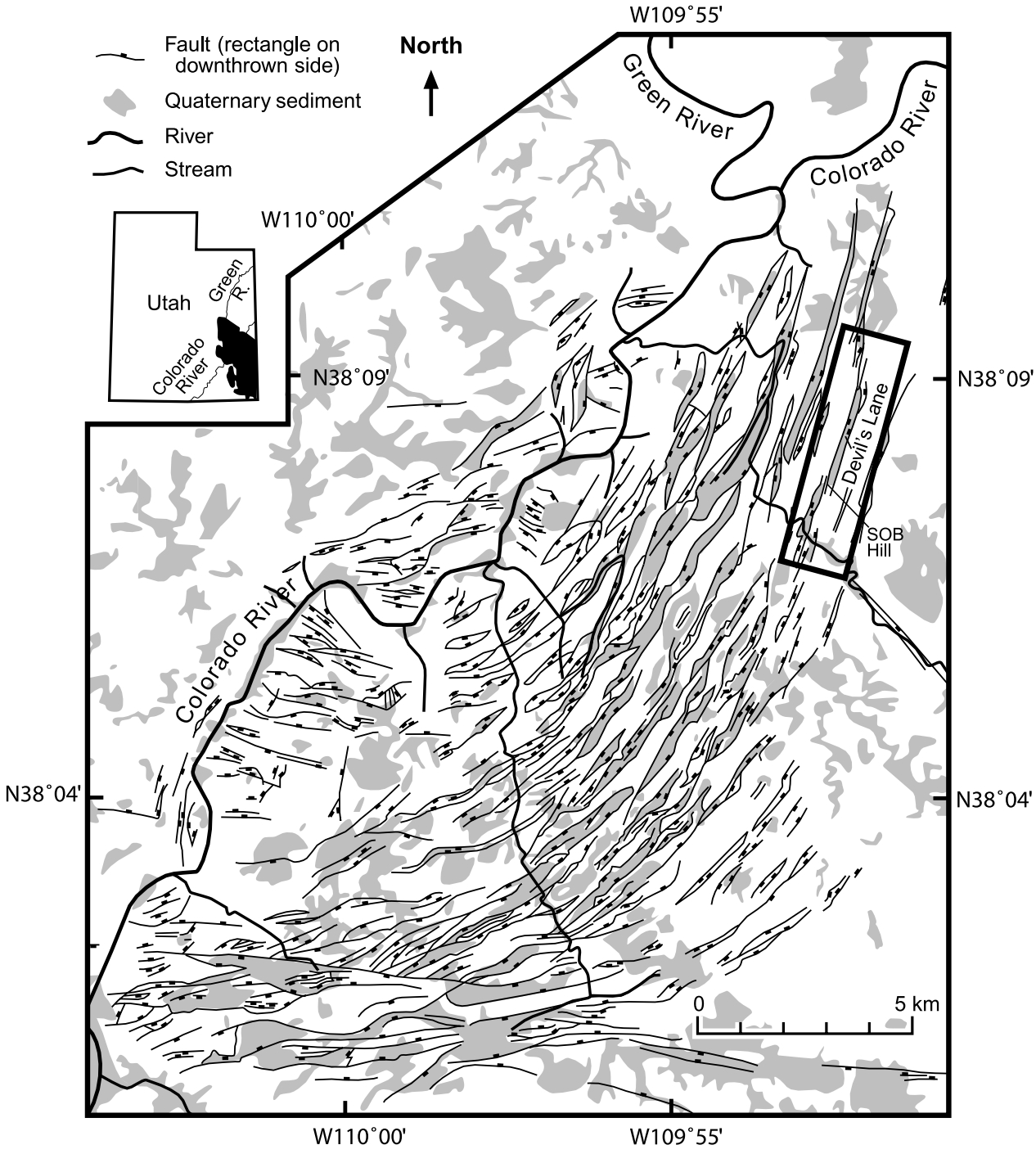

Figure 1. Map of the Needles area, Canyonlands National Park. The inset map shows the location of the park in Utah. From Schultz-Ela and Walsh (2002); reprinted with permission from Elsevier.

bands, and small faults may be difficult to identify in the relatively low-resolution cloud. Therefore, the point data were processed to generate a digital terrain model, in which far higher resolution digital imagery is draped onto triangulated surfaces generated from the point cloud (Figure 2b–e). The resulting virtual outcrop is more feasible to work with and may be used to extract spatial data such as the orientation of bedding surfaces, faults, etc. The data processing and manipulation required to generate the virtual outcrop are described in detail by Buckley et al. (2008).

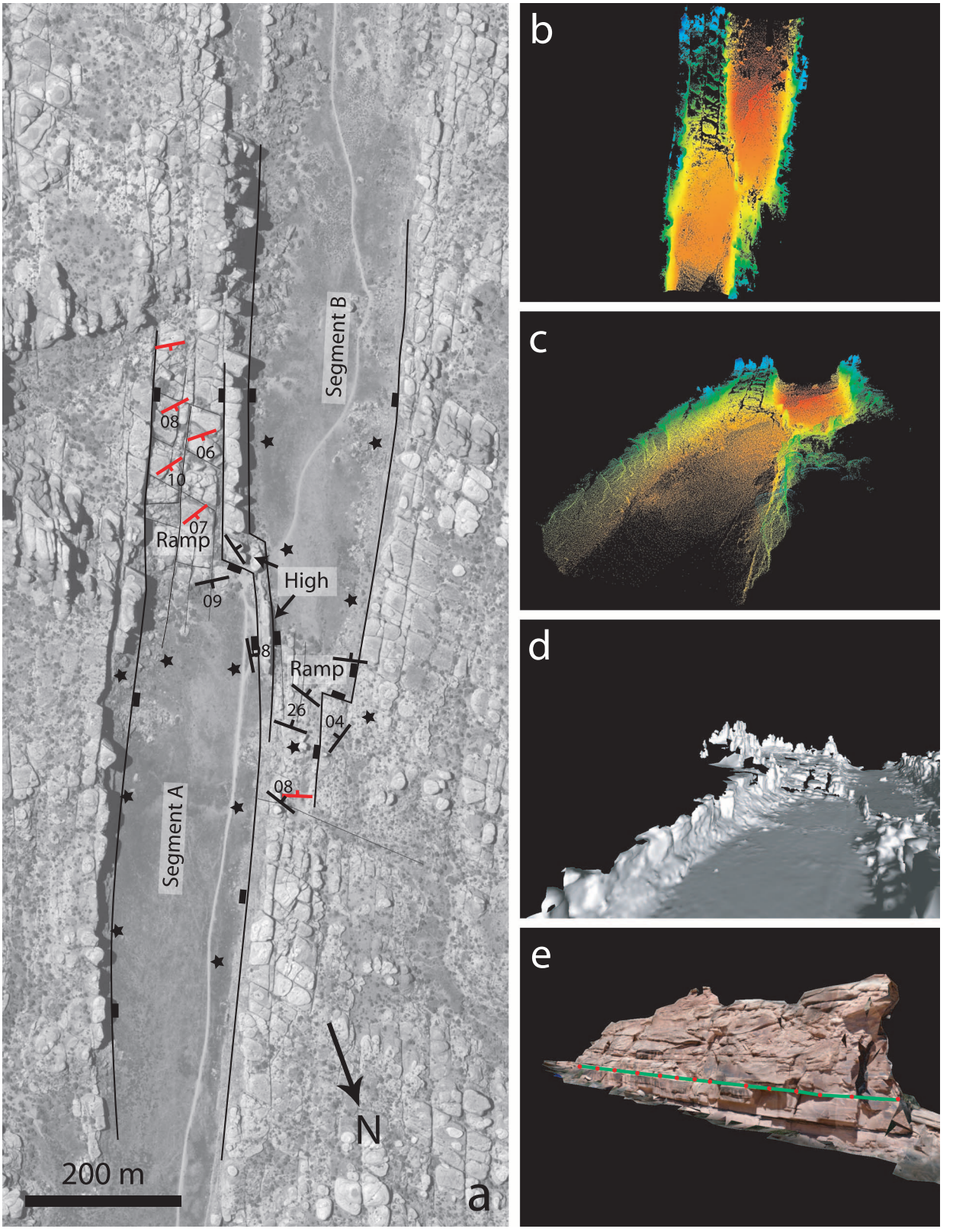

Figure 2. (a) Aerial photography of Devil's Lane. Stars mark the 13 scan locations. The red strike-slip markers were measured on the virtual outcrop, whereas the black strike-slip markers are based on field measurements. Note the right-lateral step of the graben segments. (b) Merged point cloud from LIDAR survey, birds-eye view. (c) Merged point cloud from LIDAR survey, perspective view. (d) Triangulated surface model derived from the point cloud data. (e) Part of the completed virtual outcrop, textured with high-resolution digital images. Note the digitizing of a line along a bedding surface.

Figure 3. Perspective view toward the southwest, overlooking the fault overlap zone in Devil's Lane. The graben on the right side of the picture is approximately 200 m (656 ft) wide.

Using the Virtual Outcrop to Extract Structural Geological Information

As of yet, no dedicated software is publicly available for automatically extracting geological information from the virtual outcrop. Hence, the extraction of such information is limited to (1) visual inspection of the virtual outcrop for better understanding of bed forms, correlation of beds, fracture patterns, and faults, and (2) the manual extraction of data by digitizing points and lines in the virtual outcrop (Figure 2e). The digitization of surfaces (faults, bedding etc) in the virtual outcrop is limited by outcrop exposure. Thus, the generation of a complete surface requires the use of interpolation techniques (see the next section).

In the current study, bedding plane and fault orientations were extracted from the virtual outcrop by manual digitization. The resulting orientation data for the main faults in Devil's Lane are shown graphically in Figure 4a. Orientation data from the ramp surfaces, extracted from the virtual outcrop and denoted on an aerial photo, are shown in Figure 2a. The orientation data were subsequently used to generate a 3-D geocellular model (see the Reservoir Modeling section). Other examples of structural data extracted from the virtual outcrop but not used in the subsequent reservoir model are shown in Figure 4b and c. These are shown to further exemplify the useful application of LIDAR data sets in a structural geological context.

RESERVOIR MODELING

Input from Virtual Outcrop to Reservoir Model

Current state-of-the-art reservoir modeling involves the 3-D digital representation of subsurface geology in a computer environment. Various reservoir modeling software suites exist; in the current study, the Reservoir Modeling System (RMS) version 8.0 by Roxar Software Solutions was used. This is an industry standard package and allows a complete modeling workflow from the structural modeling of faults and surfaces to the flow simulation of property-filled grids.

All main faults and a multitude of smaller faults and fractures were digitized and imported in the reservoir modeling software suite used for creating the geocellular model. Similarly, key beds were

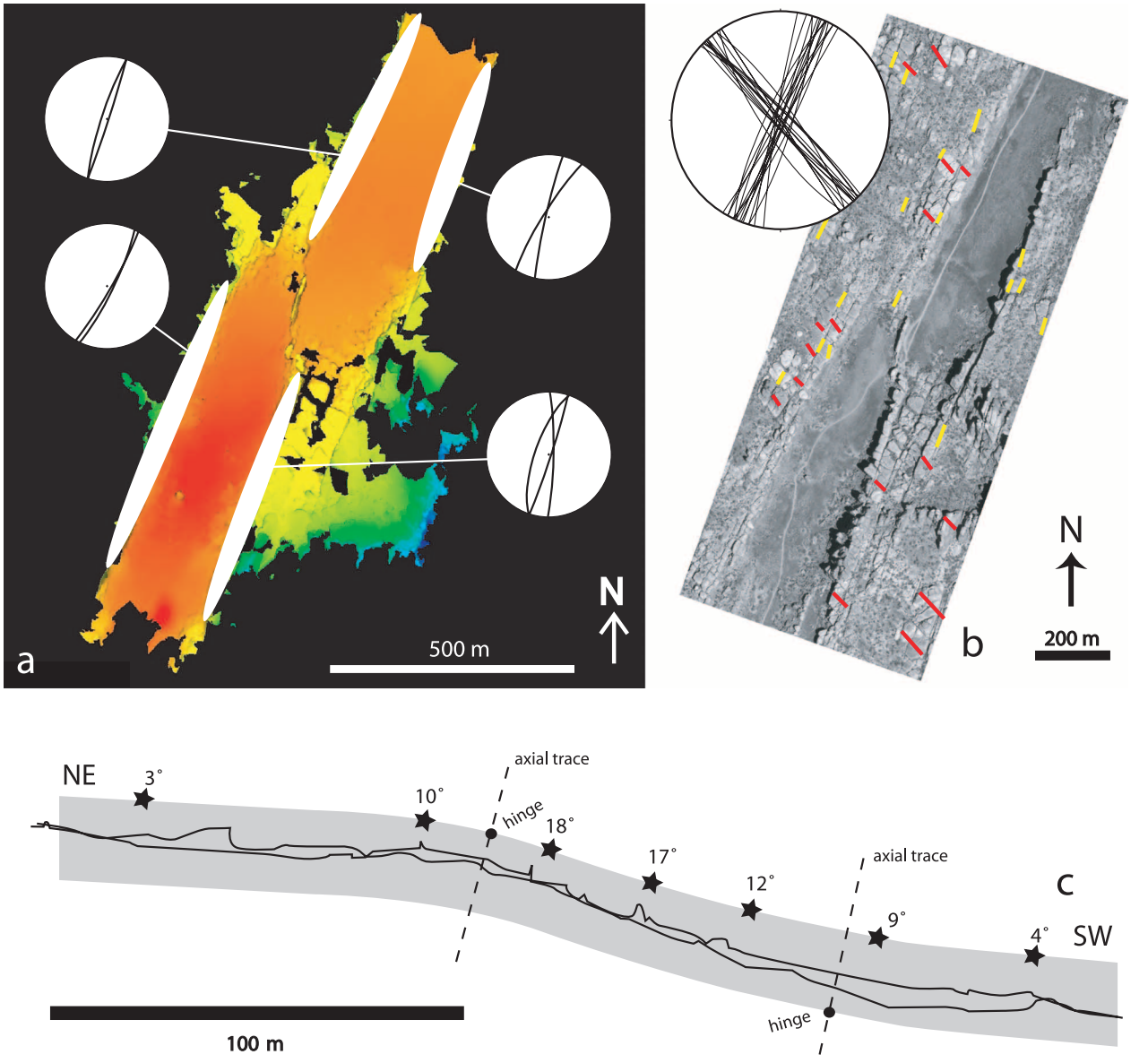

Figure 4. Structural data extracted from the virtual outcrop. (a) Equal area lower-hemisphere stereo plots of fault orientations shown on a screenshot from the RiSCAN software. (b) Equal area lower-hemisphere stereo plots of fracture orientations shown on an aerial photography of the Devil's Lane. Red and yellow lines mark the two fracture sets at high angles to each other. (c) Approximate geometry of folded beds in the northernmost relay ramp in Devil's Lane. The black lines represent the dip sections derived from the virtual outcrop on which the approximation is based. Dips of the hinges are shown and marked by stars.

digitized and imported, defining the principal stratigraphic surfaces used in the model.

Three-Dimensional Grid Generation

Based on data extracted from the virtual outcrop and imported to the reservoir modeling software, a high-quality structural framework was generated (Figure 5d, e). The stratigraphic surfaces were adjusted to the faults according to displacement, and finally, the surfaces were used to create zones and build a 3-D geological grid (Figure 5a, c). The grid should ideally be parallel to the main geological heterogeneity, and therefore, the grid was orientated to conform the orientation of the main faults. To further optimize the grid, the faults were used as guidelines, which allows the cells to be adapted to the structure by varying their X-dimension (Figure 5a).

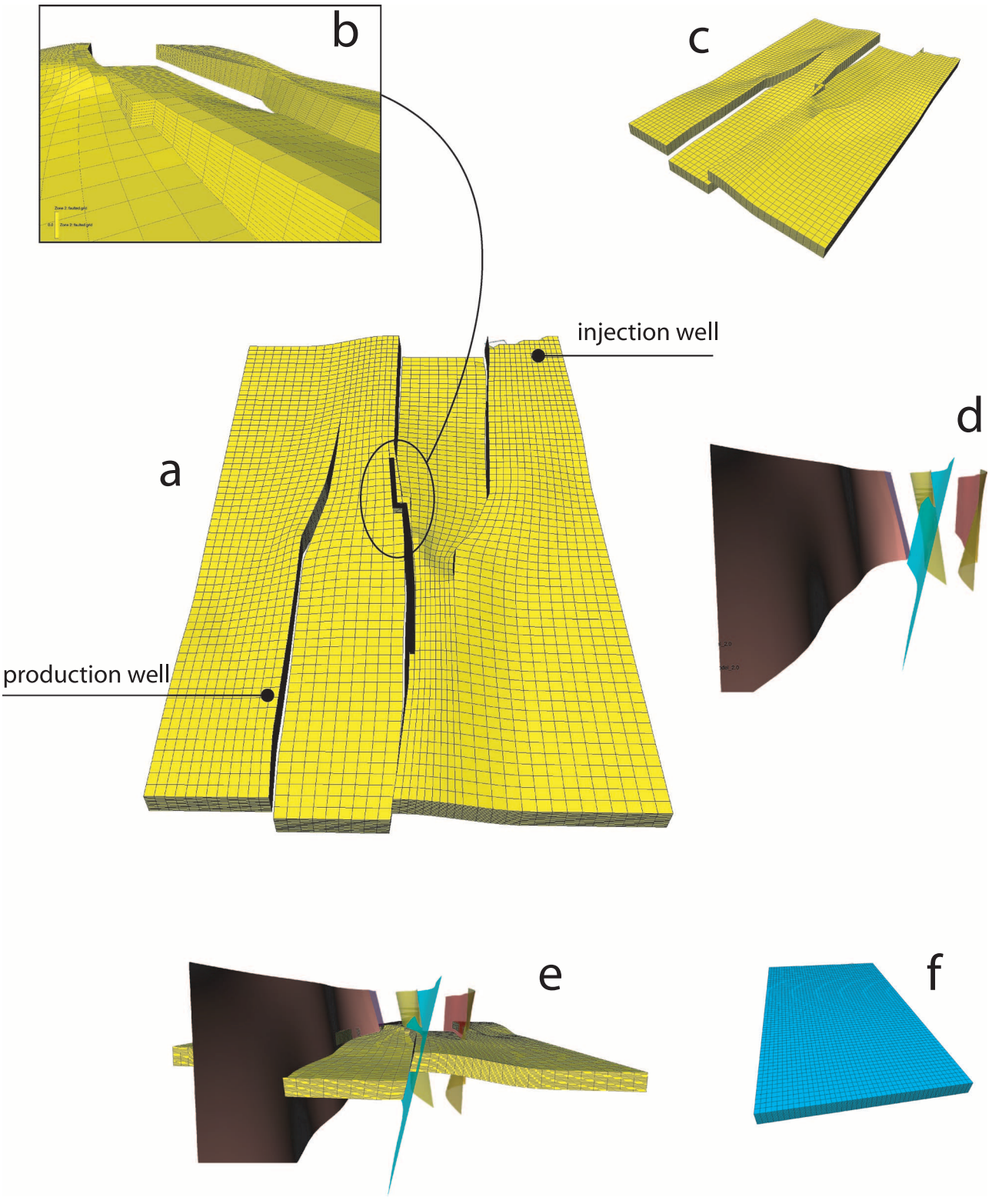

Figure 5. Three-dimensional modeling grid based on input form the virtual outcrop. (a) Faulted grid with hypothetical well locations used in fluid-flow simulations. Note the variability in the X-dimension of the cells. (b) Detail inset showing a best-approximation solution mimicking high-angle fault kinks by adapting the fault to the grid cell boundaries. (c) Perspective view of the faulted grid. (d) Fault surfaces generated in the Reservoir Modeling System. (e) Fault surfaces and faulted grid. (f) Unfaulted grid.

The model size is about 800 × 1300 × 50 m (2625 × 4265 × 164 ft), with a corresponding grid cell configuration of 44 × 65 × 20 cells, bringing the total number of cells to 57,200. This gives an average cell size of about 18 × 20 × 2.5 m (60 × 65 × 7 ft), which allows the geological detail to be captured while obviating the need for upscaling before performing fluid-flow simulation runs on the model.

In addition to the faulted 3-D geological grid, an unfaulted grid with identical dimensions was also created (Figure 5f) by removing the faults and the displacement inflicted by them. This allowed all model cases to be flow simulated (see section titled Flow Simulation) both with and without faults to isolate the effect of faulting on synthetic reservoir behavior.

In the process of fault modeling in RMS, significant efforts were initially spent trying to include a greater level of structural detail that had been extracted from the virtual outcrop (smaller faults and fractures). However, the representation of such data would have required a finer grid that would have then required upscaling, which in turn would have led to greater uncertainty in the results. Consequently, a grid resolution that was sufficiently high to satisfactorily represent the larger fault system was chosen. Excluding the extensive tension fracture system from the model is geologically justifiable because the open fractures would not be present at reservoir depths because they were formed as a response to the uplift (Moore and Schultz, 1999).

Assignment of Geological and Petrophysical Properties

The 3-D grid was populated with eight different facies models that were built to investigate the effects of the mapped structure in a variety of reservoir settings. The stratigraphy mapped and logged in the field was recreated deterministically but employing stochastic distribution of some internal facies elements. The local stratigraphy is mainly of eolian origin but also includes mudstones, limestones, and some ephemeral fluvial channel deposits (Figure 6). In addition to this deterministic model of the actual local stratigraphy, synthetic facies models were also created. This was done to investigate the effect on reservoir performance of the modeled fault system in different depositional settings. The synthetic models, representing a variety of fluvial and shallow marine environments, were generated stochastically. An overview of the facies models is shown graphically in Figure 7.

The fluvial systems were modeled using an object-based approach in which channel objects are placed stochastically in a background of overbank deposits (see Holden et al., 1998, for a description of object-based modeling of fluvial channels in RMS). These models require input on channel orientation, width, thickness, and sinuosity. Three different fluvial cases were modeled with 25, 40, and 80% channel/background ratio (net/gross). For each of the three, two separate facies models were generated, one with a depositional dip parallel to the fault system and one perpendicular to the fault system. Distributions used for drawing width, thickness, and sinuosity values from were kept constant between the models. These distributions are derived from unpublished data collected from the nonmarine deposits in the nearby Book Cliffs (see Howell and Flint, 2003, for a description of the sedimentology of this analog) and data presented in Reynolds (1999). Similarly, two shallow-marine facies models were generated, with axes of depositional dip parallel and perpendicular to the fault system, respectively. These were modeled as a series of parallel, dipping belts, which use a truncated Gaussian simulation to express facies interfingering across a linear expectation plan (see MacDonald and Aasen, 1994, for a full description of facies belt modeling in RMS). The shallow-marine facies models contain four different facies: upper shore face (USF), lower shore face (LSF), offshore transition zone (OTZ), and offshore (OFF). Belt thicknesses and degree of facies interfingering are based on the values extracted from cross sections presented by O'Byrne and Flint (1995).

In total, nine facies models were generated: one based on the actual stratigraphy, six synthetic fluvial models, and two synthetic shallow-marine models. All facies models were used to populate the faulted grid and subsequently resampled into the unfaulted grid. Thus, with one faulted and one unfaulted scenario for each facies model, 18 models were set up for the flow simulation (Figure 8; Table 1).

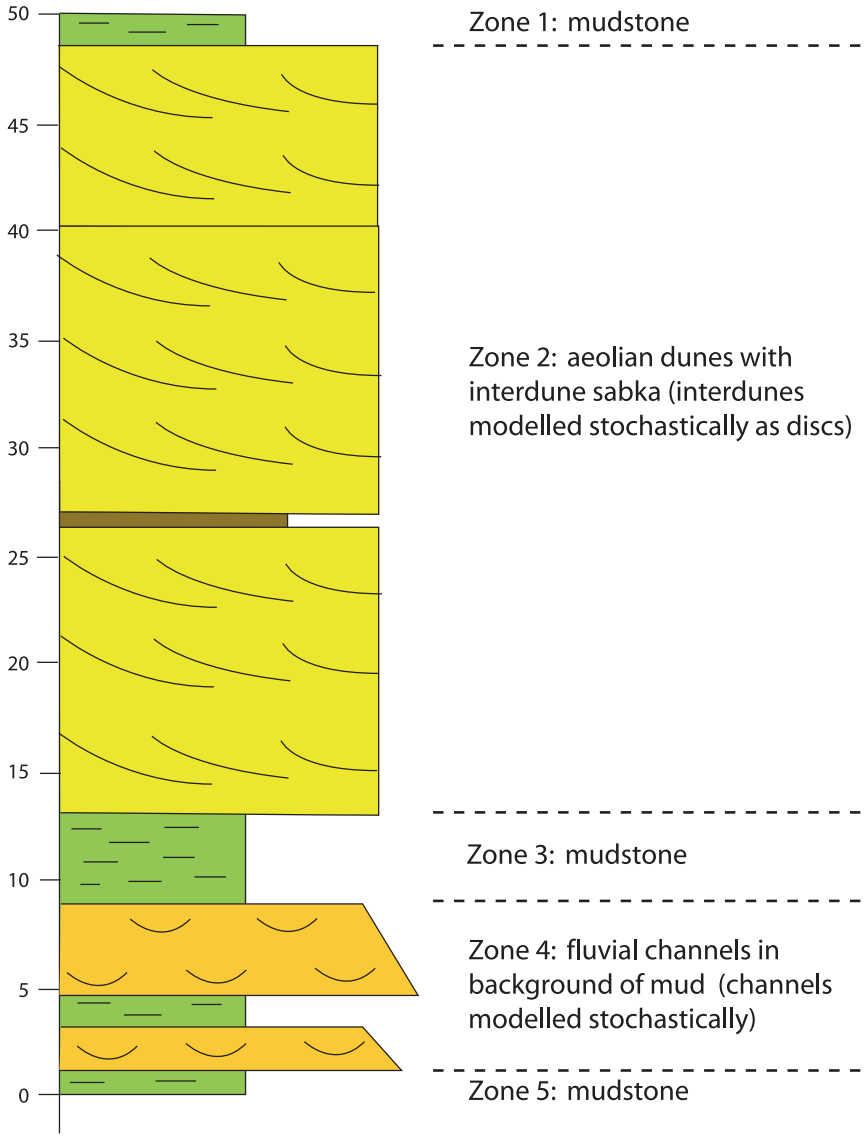

Figure 6. Schematic log of the stratigraphy as recorded in Devil's Lane. The zonation of the facies model is also shown.

As the models were built to investigate the comparative effects of facies and fault geometries on fluid flow, constant petrophysical properties were deterministically assigned on a facies by facies basis to all of the models (Skorstad et al., 2004). Stochastic procedures were not employed because these would have introduced additional noise into the results. The values used were taken from analogous North Sea fields and are summarized in Table 2. To isolate the effect of the overlapping fault geometry on fluid flow from the effects of the properties of the faults themselves (which depends on, e.g., clay smear, cataclasis, cementation, etc.), the faults were set to be completely sealing, i.e., with transmissibility equal to zero.

FLOW SIMULATION

Flow simulation was performed using the RMS finite difference, black-oil simulator. The dynamic properties used to condition the models are summarized in the Appendix. As the aim was to investigate geometric effects on flow, typical midrange properties were used and kept constant for all model runs. The flow simulations were based on a single vertical water-injection well and a single vertical production well placed on opposite sides of the faults, 1300 m (4265 ft) apart. Flow rates of 500 standard cubic meters (Sm^3)/day (3000 bbl/day) were used for both injector and producer, and a fixed bottom-hole pressure of 300 bars was set for

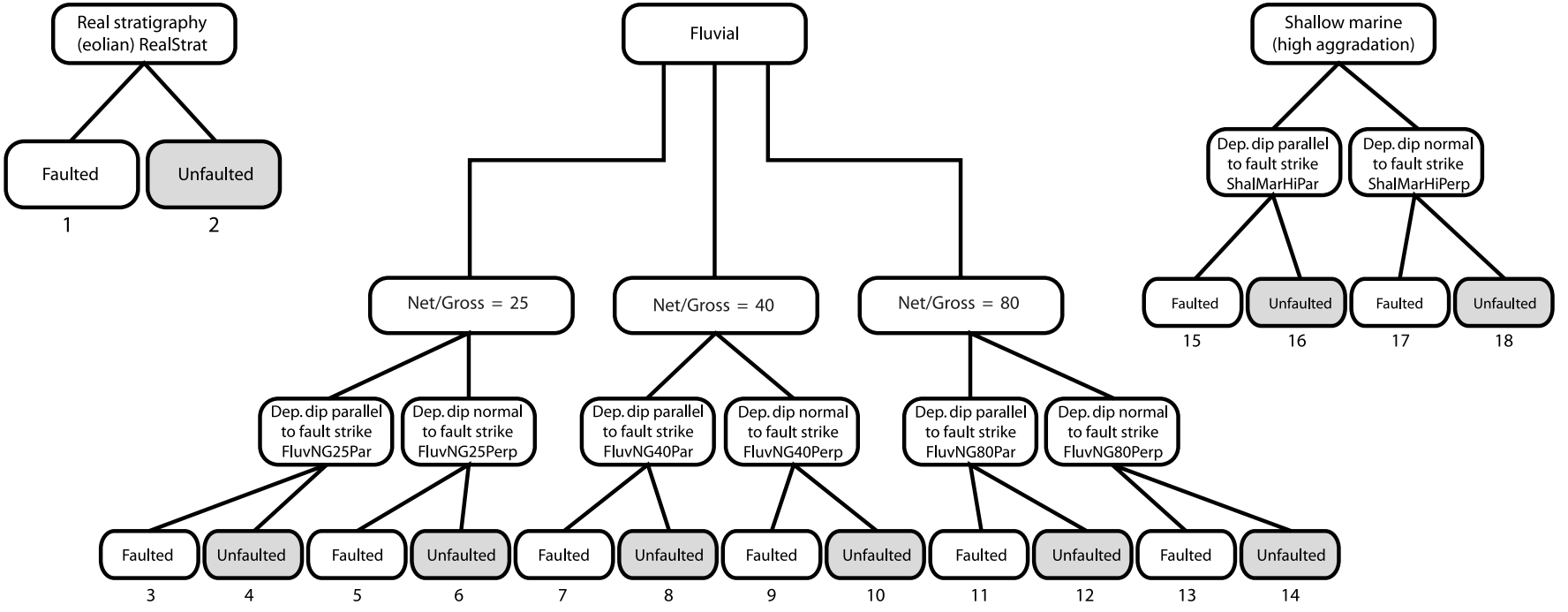

Figure 7. Hierarchic overview of the facies models created and simulated in this study. Dep. = depositional.

the injector. The simulations were run for a minimum of 10 yr or until water breakthrough occurred in the producing well. Some of the unfaulted models ran for up to 30 yr before water breakthrough occurred.

Note that the purpose of the exercise is to use flow simulation as a dynamic test of reservoir heterogeneity and to produce values that could be compared between different models. More sophisticated simulation approaches and optimization of the production are beyond the scope of this study.

EXPERIMENTAL DESIGN

Several test simulations were run to find an optimal set of dynamic properties to condition the models (mainly focusing on flow rates, oil-water contact depth, and borehole pressures). The 18 models that were built (Table 1) were then flow simulated, and the results were used to address the following issues:

1. What are the effects of the observed fault system on fluid flow if it were to occur in a subsurface hydrocarbon reservoir setting?
2. What are the effects of the fault system on fluid flow in different facies?
3. Is there a relationship between reservoir performance and the orientation of depositional dip with respect to the fault system?
4. How do the production histories of the faulted models compared to those of the unfaulted models?

Three key simulation parameters were monitored: total recovery after 10 yr of production or until water breakthrough (if this occurs after 10 yr), recovery factor, and bottom-hole pressure in the wells. The results are presented graphically (Figures 9, 10) and in table form (Table 3).

DISCUSSION

The flow-simulation results exhibit a significant spread, with total produced volumes ranging from 0.091 to 1.481 million Sm^3 (0.572 to 9.315 million bbl oil) for the faulted models, and from 1.55 to 4.936 Sm^3 (9.749 to 31.046 million bbl oil) for the unfaulted models (Figure 9a; Table 3). The relative disparity between the two populations is partly caused by a relatively large difference in stock tank oil initially in place (STOIIP, see Appendix) for faulted and unfaulted models. This is caused by the contrasting depth distribution of the model volume with regard to the oil-water contact depth. Therefore, the models are best compared by considering the recovery factor, which is scaled to STOIIP. The use of this relative parameter ensures that despite the contrasting initial in-place volumes, the production performance of the various models may be safely compared. Recovery factors range from 6.1 to 39.5% for the faulted models and from 44.3 to 65.6% for the unfaulted models (Figure 9b; Table 3). Not surprisingly, the faulted models display poorer recovery than their unfaulted equivalents, and we conclude that the faults are the most significant heterogeneity in the models. The nature and differences in which the models are affected by the faults are treated below.

Facies vs. Faults

Three depositional systems were considered: fluvial, shallow marine, and a combined eolian-fluvial system (the actual stratigraphy recorded in the field). The differential recovery factors of the faulted vs. unfaulted models are shown graphically in Figure 10b. The difference in recovery factor for the shallow-marine models is significant in both cases at 32.5 and 35.4 percentage points. For the fluvial models, the difference is also significant but more variable, with a difference in recovery factor ranging from 19.7 to 38.2 percentage points. The eolian-fluvial model features a differential recovery factor of 26.2 percentage points. Thus, the shallow-marine system appears more sensitive to the presence of faults than the other models. The fluvial models, although more variable, are also severely affected by the introduction of the fault system. The reduction of recovery is most dramatic in the models with low net/gross values and progressively less in the higher net/gross models. Thus, low net/gross systems appear to be more sensitive to the fault system than higher net/gross systems. This is explained by the more extensive channel network in a high net/

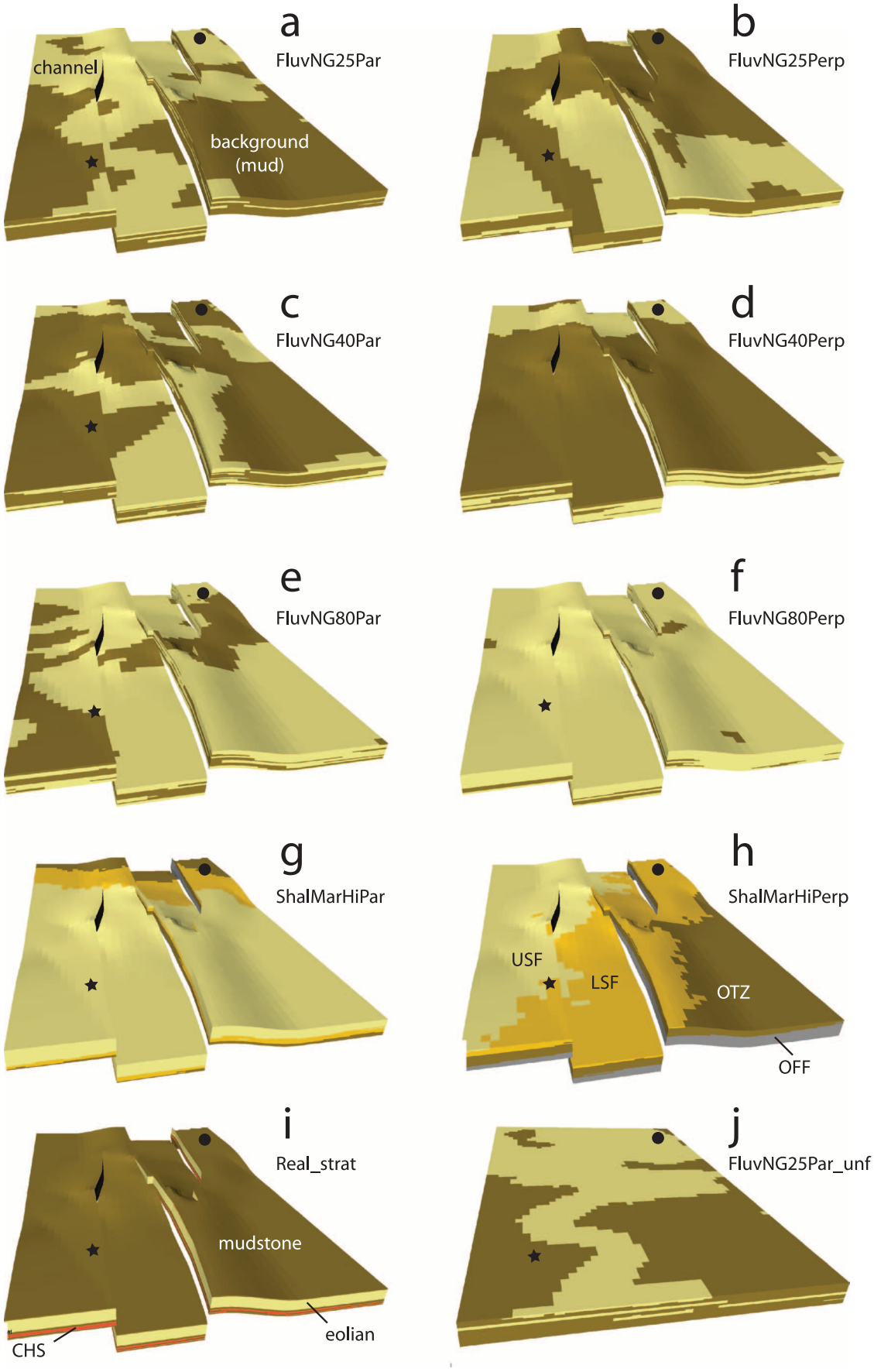
a
FluvNG25Par
channel
background
(mud)
b
FluvNG25Perp
c
FluvNG40Par
d
FluvNG40Perp
e
FluvNG80Par
f
FluvNG80Perp
g
ShalMarHiPar
h
ShalMarHiPerp
USF
LSF
OTZ
OFF
i
Real_strat
mudstone
eolian
CHS
j
FluvNG25Par_unf

Table 1. Models Built and Flow Simulated in this Study

Model Code	Facies Model	Facies Modeling Method	Depositional Dip Relative to Fault System	Grid
FluvNG25Par	Fluvial, 25% channels	Stochastic	Parallel	Faulted
FluvNG25Perp	Fluvial, 25% channels	Stochastic	Perpendicular	Faulted
FluvNG40Par	Fluvial, 40% channels	Stochastic	Parallel	Faulted
FluvNG40Perp	Fluvial, 40% channels	Stochastic	Perpendicular	Faulted
FluvNG80Par	Fluvial, 80% channels	Stochastic	Parallel	Faulted
FluvNG80Perp	Fluvial, 80% channels	Stochastic	Perpendicular	Faulted
ShalMarHiPar	Shallow marine	Stochastic	Parallel	Faulted
ShalMarHiPerp	Shallow marine	Stochastic	Perpendicular	Faulted
Real_strat	Eolian, fluvial (real stratigraphy)	Deterministic	N/A	Faulted
FluvNG25Par_unf	Fluvial, 25% channels	Stochastic	Parallel	Unfaulted
FluvNG25Perp_unf	Fluvial, 25% channels	Stochastic	Perpendicular	Unfaulted
FluvNG40Par_unf	Fluvial, 40% channels	Stochastic	Parallel	Unfaulted
FluvNG40Perp_unf	Fluvial, 40% channels	Stochastic	Perpendicular	Unfaulted
FluvNG80Par_unf	Fluvial, 80% channels	Stochastic	Parallel	Unfaulted
FluvNG80Perp_unf	Fluvial, 80% channels	Stochastic	Perpendicular	Unfaulted
ShalMarHiPar_unf	Shallow marine	Stochastic	Parallel	Unfaulted
ShalMarHiPerp_unf	Shallow marine	Stochastic	Perpendicular	Unfaulted
Real_strat_unf	Eolian, fluvial (real stratigraphy)	Deterministic	N/A	Unfaulted

gross model, making it more difficult for faults to sever communication as sand bodies are more continuous and interconnected. We also note that the higher net/gross systems produce better than the lower net/gross ones in both the faulted and unfaulted case (Figure 10a). This was anticipated and records the greater degree of connectivity. The significant reduction in performance associated with faulting both of the shallow-marine systems was initially more surprising because they represent the most continuous and sizable sand bodies. These systems are interpreted to be more sensitive to the faulting because the best quality sands (in the USF) are concentrated in a single, relatively thin continuous layer, which is determinately affected by all of the faults, whereas the sandstones in the fluvial systems are distributed evenly throughout the succession.

The eolian-fluvial system features the best recovery factor both for the faulted and the unfaulted models (Figure 10a). This is not surprising because this system represents the highest net/gross system considered in this study, and the one with the laterally most continuous sand volumes.

Orientation of Depositional Dip Axis vs. Fault-System Orientation

The orientation of the axis of depositional dip relative to the orientation of the fault system appears to have no significant bearing on production in the shallow-marine models (Figure 10a). ShalMarHiPar and ShalMarHiPerp feature similar recovery factors, as do their unfaulted equivalents. This is because the upper shoreface is a continuous sheet of sand present in both wells. For the fluvial systems, the perpendicular models produce better than the parallel models. We therefore conclude that the

Figure 8. Screenshots of the various facies models. See the text and Table 1 for details on each model. (a–i) Facies models represented in the faulted grid. Well locations are indicated by filled circles (injection well) and stars (production well). USF = upper shore face; LSF = lower shore face; OTZ = offshore transition zone; OFF = offshore; CHS = fluvial channel sands. (j) Example of facies model resampled into the unfaulted grid. FluvNG25Par_unf is the unfaulted equivalent of FluvNG25Par (a). Similarly, all other facies models were resampled into the unfaulted grid.

Table 2. Petrophysical Values used for Input to the Fluid-Flow Simulation

Facies	Horizontal Permeability (md)	Vertical Permeability (md)	Porosity (%)
Fluvial			
Channel	500	100	20
Background (clay or mud)	1	0.1	5
Shallow marine			
USF (upper shoreface)	200	50	20
LSF (lower shoreface)	100	20	15
OTZ (offshore transition zone)	50	1	12
OFF (offshore)	1	0.1	5
Real stratigraphy			
Mudstone	0.1	0.01	5
Eolian sand	1000	500	30
Interdune sabka	100	50	16
Fluvial channel	400	100	20

orientation of the axis of depositional dip relative to the fault system orientation is an important factor to consider in fluvial systems. Particularly for the low net/gross models, the localization and orientation of channels and the severing of these by faulting may be critical to production because of the low ratio of channel sands to mud.

Pressure Communication

Pressure communication across the overlapping fault system is extremely poor. This is manifested by an immediate decrease in the bottom-hole pressure in the producer and a coeval immediate increase in bottom-hole pressure in the injector once the production starts (Figure 11). This shows that although the presence of relay zones in the area of fault overlap allows fluids to cross the fault system, compartmentalization is nevertheless significant. The volumes extracted at the production well obviously far exceed the volumes of fluids crossing the overlap zone, with a resulting large pressure difference between the two compartments. This is an important result because overlap zones and relay ramps are generally considered conduits for flow in subsurface reservoirs. Although this is true in terms of providing a pathway for limited fluid flow between otherwise breached reservoir zones, compartmentalization in terms of poor pressure communication may still be preserved. Therefore, sealing faults may retain their negative effect on fluid-flow communication also in the presence of soft-linked relays.

Use of LIDAR

The use of LIDAR data to construct an outcrop model of a structurally complex reservoir analog has in this study been successful. The virtual outcrop constructed based on LIDAR data was used as input to build the model. Other important structural data were also extracted from the virtual outcrop, although limitations exist. The main limitation is the dependency on outcrop quality and exposure of structures. The extraction of structural data in this study was aided by optimal exposure of fault surfaces, fracture systems, and bedding surfaces such as the relay ramps. Using LIDAR data

Table 3. Summary of Flow Simulation Results

Model Code	Total Production (million m^3)	Recovery Factor (%)	Length of Run (yr)
FluvNG25Par	0.091	6.1	10
FluvNG25Perp	0.175	12.6	10
FluvNG40Par	0.47	25.1	10
FluvNG40Perp	0.55	29.6	10
FluvNG80Par	0.935	37.1	10
FluvNG80Perp	1.116	39.5	10
ShalMarHiPar	0.416	19.5	10
ShalMarHiPerp	0.317	16.9	10
Real_strat	1.481	39.4	10
FluvNG25Par_unf	1.55	44.3	10
FluvNG25Perp_unf	1.5	46.9	10
FluvNG40Par_unf	2.405	53.9	15
FluvNG40Perp_unf	2.53	54.1	15
FluvNG80Par_unf	3.431	56.8	20
FluvNG80Perp_unf	4.033	61.5	25
ShalMarHiPar_unf	2.423	52	15
ShalMarHiPerp_unf	2.135	52.3	15
Real_strat_unf	4.936	65.6	30

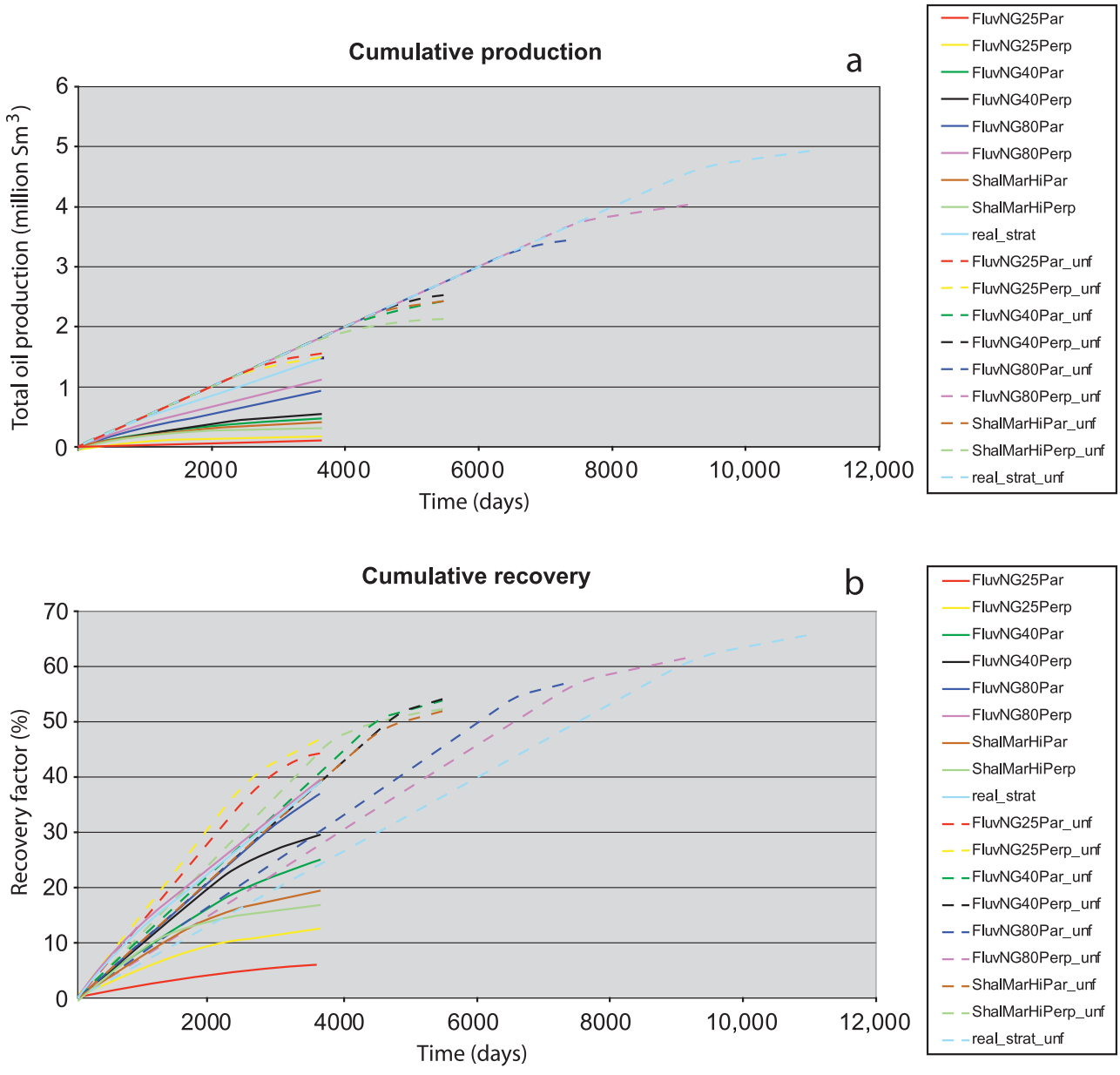

Figure 9. Flow simulation results. Note that the total run time is variable as the models were simulated for a minimum of 10 yr or until water breakthrough. (a) Cumulative production over time. (b) Cumulative recovery over time. Sm^3 = standard cubic meters.

to extract structural data from outcrops where the structures are less exposed would prove problematic. Thus, we conclude that the use of this technology in a structural setting is both time efficient and useful but dependent on good exposure of structural elements. However, developing automated tools for geological and structural analysis, i.e., for recognizing fractures, automated strike-dip tools, etc., would be useful and would make the use of LIDAR technology even more interesting to geologists.

SUMMARY AND CONCLUSIONS

Based on the outcrop modeling and fluid-flow simulation studies presented herein, the following conclusions were drawn:

1. The models without the fault network achieved significantly greater recovery factors than the faulted models. The fault system represents the most significant heterogeneity in the models.

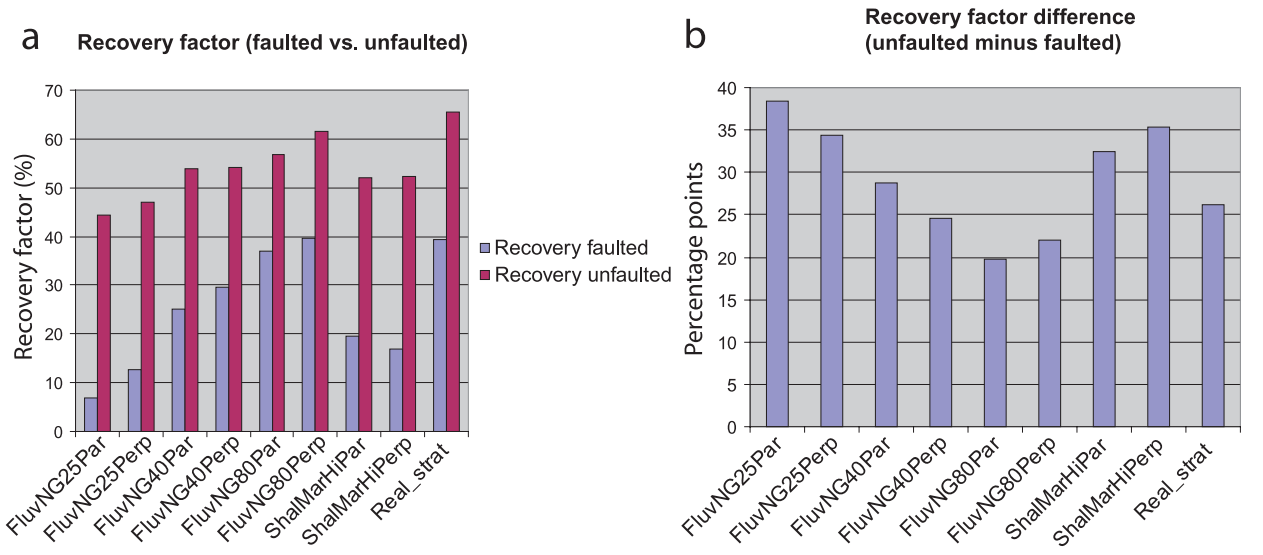

Figure 10. Comparative results for recovery factors at the end of all simulation runs. (a) Recovery factor results comparing the faulted facies models to their unfaulted equivalents. (b) Differential recovery factor (recovery factor of the unfaulted facies model minus recovery factor of the faulted model).

2. Production in reservoirs formed in different depositional systems respond differently to the faulting. The fault system had the most negative effect on production in the shallow-marine and low net/gross fluvial models when compared to unfaulted equivalents. Furthermore, production in low net/gross fluvial systems appeared to be more negatively affected by the fault system than higher net/gross fluvial systems. The eolian-fluvial (real) stratigraphy featured the highest recovery factors, both for unfaulted and faulted models, because of the extent and lateral continuity of sand bodies.
3. Models with matching facies but varying orientation of the axis of depositional dip relative to the fault system were compared. The results indicated that, in fluvial systems, the effects on production imposed by the fault system were dependent on the orientation of the depositional dip axis relative to the faults; specifically, fluvial models with perpendicular depositional dips produced more efficiently. A similar dependency was not seen in the shallow-marine models.
4. Pressure data indicated that, although fluids did flow across the overlap zone, pressure communication across the fault system was extremely poor. Large pressure differences between the two main compartments were recorded. Dependent on dimensions, relay zones may thus act as a

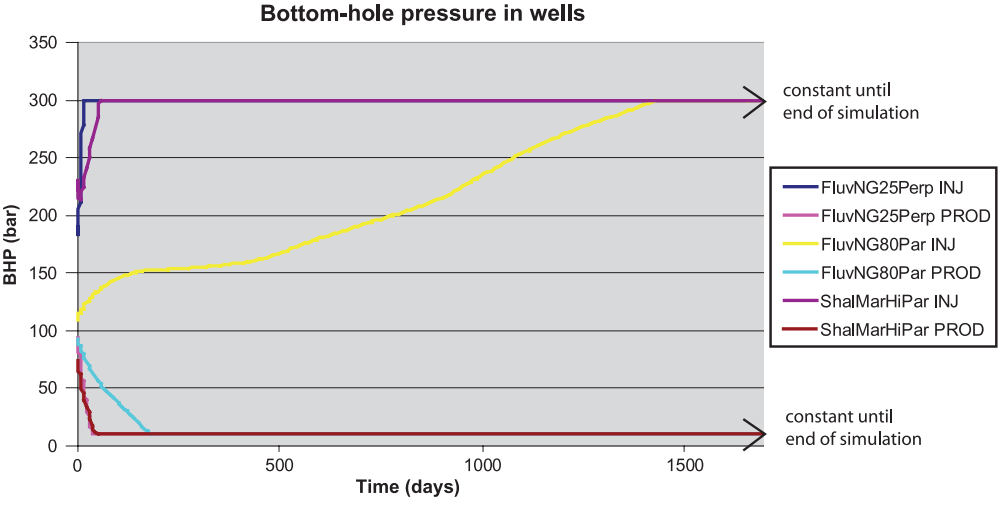

Figure 11. Bottom hole pressure (BHP) in injection and production wells of faulted models. Note the difference in BHP between injection and production wells for the three examples shown, indicating extremely poor pressure communication between the wells.

conduit for limited fluid flow between otherwise breached reservoir zones but may still not provide sufficient communication for pressures to be equalized between compartments. This would cause the effects of well injection on one side of the fault system to be minimal on the other side. This is an important conclusion for relay ramps because they are generally considered to preserve communication between compartments because of the geometric connectivity associated with the soft-linked fault overlap. As this study shows, however, such geometric connectivity may be insufficient to achieve pressure communication across faults.

5. In addition to the geological implications of this study, we have demonstrated a methodology for field data collection and outcrop modeling using LIDAR technology as a basis for the generation of a structurally complex analogous reservoir model.

APPENDIX: FLOW SIMULATION DYNAMIC PROPERTIES

Minimum length of run	10 yr		
Other run constraints	Production until water breakthrough		
Report step	1 quarter		
Rock compressibility	0.0000435 1/bar		
Rock reference pressure	275.79 bar		
Specific gravity oil	0.8		
Gas/oil ratio	142.486 Sm^3/Sm^3		
Corey exponents	Water	4	
	Oil-water	3	
Saturation end points	Sorw	0.2	
	Swcr	0.2	
Relative permeability end points	kromax	1	
	krw	0.4	
Top of model	Faulted grid	1335 m	
	Unfaulted grid	1338 m	
Oil-water contact	Faulted grid	1380 m	
	Unfaulted grid	1400 m	
Oil-water contact capillary pressure	0		
Reference depth	1400 m		
Reference pressure	100 bar		
Wells	Injectors	1	
	Producers	1	
Flow rate	Injector	500 Sm^3/day	
	Producer	500 Sm^3/day	
Bottom-hole pressure	Injectors	300 bar	
Initial oil in place	Faulted grid	FluvNG25Par	1,480,752 Sm^3
		FluvNG25Perp	1,390,337 Sm^3
		FluvNG40Par	1,870,835 Sm^3
		FluvNG40Perp	1,860,414 Sm^3
		FluvNG80Par	2,518,996 Sm^3
		FluvNG80Perp	2,823,905 Sm^3
		ShalMarHiPar	2,138,992 Sm^3
		ShalMarHiPerp	1,878,509 Sm^3
		Real_strat	3,762,309 Sm^3
	Unfaulted grid	FluvNG25Par_unf	3,497,857 Sm^3
		FluvNG25Perp_unf	3,199,760 Sm^3
		FluvNG40Par_unf	4,464,428 Sm^3
		FluvNG40Perp_unf	4,674,539 Sm^3
		FluvNG80Par_unf	6,038,572 Sm^3
		FluvNG80Perp_unf	6,562,566 Sm^3
		ShalMarHiPar_unf	4,660,403 Sm^3
		ShalMarHiPerp_unf	4,082,389 Sm^3
		Real_strat_unf	8,219,921 Sm^3

REFERENCES CITED

Baars, D. R., 2003, Geology of Canyonlands National Park, Utah, *in* D. A. Sprinkel, T. C. J. Chidsey, and P. B. Anderson, eds., Geology of Utah's parks and monuments: Utah Geological Association Publication 28: Salt Lake City, Utah Geological Association and Bryce Canyon Natural History Association, p. 61–83.

Bellian, J. A., C. Kerans, and D. C. Jenette, 2005, Digital outcrop models: Application of terrestrial scanning LIDAR technology in stratigraphic modeling: Journal of Sedimentary Research, v. 75, p. 166–176.

Bryant, I., D. Carr, P. Cirilli, N. Drinkwater, D. McCormick, P. Tilke, and J. Thurmond, 2000, Use of 3D digital analogs as templates in reservoir modeling: Petroleum Geoscience, v. 6, p. 195–201.

Buckley, S. J., J. A. Howell, H. D. Enge, and T. H. Kurz, 2008, Terrestrial laser scanning in geology: Data acquisition, processing and accuracy considerations: Journal of the Geological Society (London), v. 165, p. 625–638.

Cartwright, J. A., C. S. Mansfield, and B. D. Trudgill, 1996, Fault growth by segment linkage, *in* P. C. Buchanan and D. A. Nieuwland, eds., Modern developments in structural interpretations: Geological Society (London) Special Publication 99, p. 163–177.

Childs, C., J. Watterson, and J. J. Walsh, 1995, Fault overlap zones within developing normal fault systems: Journal of the Geological Society (London), v. 152, p. 535–549.

Clegg, P., I. Trinks, K. J. W. McCaffrey, R. E. Holdsworth, R. R. Jones, R. Hobbs, and S. Waggot, 2005, Toward the virtual outcrop: Geoscientist, v. 15, p. 8–9.

Davis, G. H., 1999, Structural geology of the Colorado Plateau region of southern Utah, with special emphasis on deformation bands: Geological Society of America Special Paper 342, 157 p.

Dreyer, T., L. M. Falt, T. Hoy, R. Knarud, R. Steel, and J. L. Cuevas, 1993, Sedimentary architecture of field analogs for reservoir information (SAFARI), a case study of the fluvial Escanilla Formation, Spanish Pyrenees, *in* S. S. Flint and I. D. Bryant, eds., The geological modeling of hydrocarbon reservoirs and outcrop analogs: Special Publication of the International Association of Sedimentologists 15, p. 57–80.

Enge, H. D., S. J. Buckley, A. Rotevatn, and J. A. Howell, 2007, From outcrop to reservoir simulation model: Workflow and procedures: Geosphere, v. 3, p. 469–490.

Fisher, Q. J., and R. J. Knipe, 2001, The permeability of faults within siliciclastic petroleum reservoirs of the North Sea and Norwegian Continental Shelf: Marine and Petroleum Geology, v. 18, p. 1063–1081.

Flint, S. S., and I. Bryant, 1993, The geological modeling of hydrocarbon reservoirs and outcrop analogs: Special Publication of the International Association of Sedimentologists 15: Oxford, Blackwell Scientific Publications, 249 p.

Grammer, M. G., and G. P. Eberlli, eds., 2004, Integration of outcrop and modern analogs in reservoir modeling: AAPG Memoir 80, 396 p.

Hesthammer, J., and H. Fossen, 1997, Seismic attribute analysis in structural interpretation of the Gullfaks field, northern North Sea: Petroleum Geoscience, v. 3, p. 13–26.

Hodgetts, D., N. J. Drinkwater, D. Hodgson, J. Kavanagh, S. S. Flint, K. J. Keogh, and J. A. Howell, 2004, Three-dimensional geological models from outcrop data using digital data collection techniques: An example from the Tanqua Karoo depocenter, South Africa, *in* A. Curtis and R. Wood, eds., Geological prior knowledge: Geological Society (London) Special Publication 239, p. 57–75.

Holden, L., R. Hauge, O. Skare, and A. Skorstad, 1998, Modeling of fluvial reservoirs with object models: Mathematical Geology, v. 30, p. 473–496.

Howell, J. A., and S. S. Flint, 2002, Application of sequence stratigraphy in production geology and 3-D reservoir modeling: Gulf Coast Section SEPM, v. 21, p. 633–645.

Howell, J. A., and S. S. Flint, 2003, Sequences and systems tracts in the Book Cliffs, *in* A. Coe, ed., The sedimentary record of sea level change: Cambridge, United Kingdom, Cambridge University Press, p. 179–197.

Howell, J. A., Å. Vassel, and T. Aune, in press, Modeling of dipping clinoform barriers within deltaic outcrop analogs from the Cretaceous Western Interior Basin U.S.A.: Geological Society (London) Special Publication.

Knipe, R. J., 1997, Juxtaposition and seal diagrams to help analyze fault seals in hydrocarbon reservoirs: AAPG Bulletin, v. 81, p. 187–195.

Levoy, M., et al., 2000, The Digital Michelangelo Project: 3-D scanning of large statues: Proceedings of the 27th Annual Conference on Computer Graphics and Interactive Techniques, p. 131–144.

MacDonald, A. C., and J. O. Aasen, 1994, A prototype procedure for stochastic modeling of facies tract distribution in shoreface reservoirs, *in* J. M. Yarus and R. L. Chambers, eds., Stochastic modeling and geostatistics: Principles, methods, and case studies: AAPG Computer Application in Geology 3, p. 91–108.

Mansfield, C. S., and J. A. Cartwright, 2001, Fault growth by linkage: Observations and implications from analog models: Journal of Structural Geology, v. 23, p. 745–763.

Manzocchi, T., A. E. Heath, J. J. Walsh, C. Childs, and W. R. Bailey, 2004, Faults in conventional flow models: An investigation of numerical and geological assumptions: Annex 8 of the Final Technical Report for the SAIGUP Project, European Union project no. NNE5-2000-20095, 17 p.

McCaffrey, K. J. W., R. R. Jones, R. E. Holdsworth, R. W. Wilson, P. Clegg, J. Imber, N. Holliman, and I. Trinks, 2005, Unlocking the spatial dimension: Digital technologies and the future of geoscience fieldwork: Journal of the Geological Society (London), v. 162, p. 927–938.

Moore, J. M., and R. A. Schultz, 1999, Processes of faulting in jointed rocks of Canyonlands National Park, Utah: Geological Society of America Bulletin, v. 111, p. 808–822.

Mountney, N. P., 2004, Stratigraphic evolution of an eolian erg margin system, the Permian Cedar Mesa Sandstone, SE Utah, U.S.A.: Sedimentology, v. 51, p. 713–743.

O'Byrne, C. J., and S. S. Flint, 1995, Sequence, parasequence and intraparasequence architecture of the Grassy Member, Blackhawk Formation, Book Cliffs, Utah, U.S.A.,

in J. C. Van Wagoner and G. T. Bertram, eds., Sequence stratigraphy of foreland basin deposits: AAPG Memoir 64, p. 225–257.

Peacock, D. C. P., and D. J. Sanderson, 1991, Displacements, segment linkage and relay ramps in normal fault zones: Journal of Structural Geology, v. 13, p. 721–733.

Peacock, D. C. P., and D. J. Sanderson, 1994, Geometry and development of relay ramps in normal fault systems: AAPG Bulletin, v. 78, p. 147–165.

Pringle, J., A. Gardiner, and R. Westerman, 2004a, Virtual geological outcrops-fieldwork and analysis made less exhaustive?: Geology Today, v. 20, p. 67–72.

Pringle, J. K., A. R. Westerman, J. D. Clark, N. J. Drinkwater, and A. R. Gardiner, 2004b, 3-D high-resolution digital models of outcrop analog study sites to constrain reservoir model uncertainty: An example from Alport Castles, Derbyshire, United Kingdom: Petroleum Geoscience, v. 10, p. 343–352.

Pringle, J. K., J. A. Howell, D. Hodgetts, A. R. Westerman, and D. M. Hodgson, 2006, Virtual outcrop models of petroleum reservoir analogs: A review of the current state-of-the-art: First Break, v. 24, p. 33–42.

Reynolds, A. D., 1999, Dimensions of paralic sandstone bodies: AAPG Bulletin, v. 83, p. 211–229.

Rotevatn, A., H. Fossen, J. Hesthammer, T. E. Aas, and J. A. Howell, 2007, Are relay ramps conduits for fluid flow? Structural analysis of a relay ramp in Arches National Park, Utah, *in* L. Lonergan, R. J. H. Jolly, D. J. Sanderson, and K. Rawnsley, eds., Fractured reservoirs: Geological Society (London) Special Publication 270, p. 55–71.

Sagy, A., E. E. Brodsky, and G. J. Axen, 2007, Evolution of fault-surface roughness with slip: Geology, v. 35, p. 283–286.

Schultz-Ela, D. D., and P. Walsh, 2002, Modeling of grabens extending above evaporites in Canyonlands National Park, Utah: Journal of Structural Geology, v. 24, p. 247–275.

Skorstad, A., O. Kolbjørnsen, B. Fjellvoll, J. A. Howell, T. Manzocchi, and J. N. Carter, 2004, Sensitivity of oil production to petrophysical heterogeneities, *in* O. Leuangthong and C. V. Deutsch, eds., Geostatistics Banff 2004: Dordrecht, Netherlands, Springer, v. 2, p. 723–730.

Sorkhabi, R., and Y. Tsuji, eds., 2005, Faults, fluid flow and petroleum traps: AAPG Memoir 85, 342 p.

Trudgill, B. D., and J. A. Cartwright, 1994, Relay ramp forms and normal fault linkages, Canyonlands National Park, Utah: Geological Society of America Bulletin, v. 106, p. 1143–1157.

Waggot, S., P. Clegg, and R. R. Jones, 2005, Combining terrestrial laser scanning, RTK GPS and 3-D visualization: Application of optical 3-D measurement in geological exploration: Proceedings of the 7th Conference on 3-D Optical Measurement Techniques: http://www.dur.ac.uk/react.res/RRG_web/pdf/publications/waggot.pdf.

Wilson, R. W., K. J. W. McCaffrey, R. R. Jones, J. Imber, P. Clegg, and R. E. Holdsworth, 2005, Lofoten has its faults! Detailed fault analysis and 3-D digital mapping in the Norway's Lofoten Islands: Geoscientist, v. 15, p. 4–9.